Journal of
Synchrotron
Radiation

ISSN 0909-0495

Received 22 September 2010
Accepted 4 November 2010

Adaption of a diffractometer for time-resolved X-ray resonant magnetic scattering

Stefan Buschhorn,* Frank Brüssing, Radu Abrudan and Hartmut Zabel

Institut für Experimentalphysik/Festkörperphysik, Ruhr-Universität Bochum, 44780 Bochum, Germany. E-mail: stefan.buschhorn@ruhr-uni-bochum.de

A new set-up is presented to measure element-selective magnetization dynamics using the ALICE chamber [Grabis *et al.* (2003), *Rev. Sci. Instrum.* **74**, 4048–4051] at the BESSY II synchrotron at the Helmholtz-Zentrum Berlin. A magnetic-field pulse serves as excitation, and the magnetization precession is probed by element-selective X-ray resonant magnetic scattering. With the use of single-bunch-generated X-rays a temporal resolution well below 100 ps is reached. The ALICE diffractometer environment enables investigations of thin films, described here, multilayers and laterally structured samples in reflection or diffuse scattering geometry. The combination of the time-resolved set-up with a cryostat in the ALICE chamber will allow temperature-dependent studies of precessional magnetization dynamics and of damping constants to be conducted over a large temperature range and for a large variety of systems in reflection geometry.

Keywords: precession; magnetization dynamics; magnetic nanostructures; time-resolved resonant magnetic X-ray scattering.

1. Introduction

Nanomagnetism on short time scales has attracted much interest in recent years for both a fundamental understanding and for technological reasons. The time scales reach from seconds for fluctuations of magnetization in nanoparticles and ultrathin films (Wernsdorfer *et al.*, 1997; Shpyrko *et al.*, 2007), microseconds to nanoseconds for magnetization reversal processes *via* domain wall motion (Kläui, 2008), picoseconds for precessional dynamics (Kalarickal *et al.*, 2006), to femtoseconds for demagnetization processes *via* heat pulses (Beaurepaire *et al.*, 1996; Stamm *et al.*, 2007; Dürr *et al.*, 2009). The precessional dynamics that occurs in response to a change of the external magnetic field direction is of particular interest as it constitutes the basic step to a complete magnetization reversal. The damped precessional motion about the new field direction is entirely governed by the Landau–Lifshitz–Gilbert equation. The precessional dynamics can be studied either by driving the ferromagnetic system into resonance *via* microwave excitation (FMR) (Farle, 1998; Heinrich, 2008), where the width of the resonance line is a measure of the damping constant, or in real time *via* a step or impulse excitation, where the system subsequently relaxes into the effective field direction with a characteristic time constant (Nibarger *et al.*, 2003; Silva *et al.*, 1999). While FMR experiments on nanomagnetic systems are well established (Bland & Heinrich, 2005), pulse field excitation experiments are less common. Pioneering work was carried out by Silva and Gerrits using an Auston switch for generating a strong current pulse, which, in turn, produces a magnetic field pulse within the sample (Gerrits *et al.*, 2002, 2006). Using the time-resolved magneto-optical Kerr effect (Bauer *et al.*, 2000; Neudert *et al.*, 2005; Hubert & Schäfer, 1998) the precessional switching can be resolved in real time. For magnetic alloys and for magnetic heterostructures it is desirable to have a method which not only has sufficient time resolution but also provides element-selective information. For domain wall and vortex dynamics, time-resolved photoemission electron microscopy (tr-PEEM) (Kaiser *et al.*, 2009; Vogel *et al.*, 2003; Raabe *et al.*, 2005) and time-resolved scanning transmission X-ray microscopy (Bocklage *et al.*, 2008; Van Waeyenberge *et al.*, 2006) experiments are powerful element-selective tools using resonant absorption.

Time-resolved X-ray resonant magnetic scattering (tr-XRMS) combines the advantages of resonant magnetic X-ray scattering, *i.e.* reflection geometry, depth and interface sensitivity, high magnetic field and low-temperature application, with probing of the element-specific precessional motion. Therefore, issues such as choice of substrate, film thickness and surface contamination are less severe. Furthermore, tr-XRMS lends itself to the study of depth and layer-resolved precessional dynamics in thin films, magnetic heterostructures and magnetic multilayers. It has been demonstrated for the first time by Bailey *et al.* (2004) in the time domain and in reflection geometry at fixed incident angle. These experiments were later accompanied by transition geometry experiments with FMR (Arena *et al.*, 2009; Martin *et al.*, 2009) and pulsed excitation (Martin *et al.*, 2008).

Here we describe a newly developed tr-XRMS set-up that allows excitation of nanomagnetic systems using field pulses on the 100 ps time scale. The free precessional response as well as the precessional damping over several nanoseconds is then followed for each element by tuning the photon energy to the different X-ray resonance absorption edges. This real-time method also enables us to address the low-frequency limit of precessional motion that is still challenging in the frequency domain. The diffractometer environment enables measurements at variable incident angle in order to study q-dependent profiles of the magnetization dynamics. Thereby depth-dependent phenomena like standing spin waves or helical magnetization systems can be investigated. In the following we first describe the experimental set-up of our system and then provide preliminary results from a $Fe_{20}Ni_{80}$ (Py) thin-film sample.

2. Experimental set-up

In our set-up we combine the element-selective technique of XRMS with the pulsed structure of the X-rays provided by a synchrotron storage ring in order to enable time-resolved experiments, as depicted in Fig. 1.

The sample is excited by a magnetic field pulse, and after a fixed delay the instant magnetization is probed by the X-ray pulse. By controlling the delay between pump and probe in steps as small as 10 ps we monitor the instant magnetization at fixed times after the onset of the excitation. The resulting delay scan yields an element- and time-resolved sequence of the precessional dynamics in the sample. We emphasize that tr-XRMS measures the coherent dynamics of individual magnetic moments in variable magnetic fields in a fast and direct way. This can be done *via* PEEM experiments as well (Raabe *et al.*, 2005); however, in most publications using element-selective techniques the authors concentrate on the dynamics of domain structures like Landau patterns (Kaiser *et al.*, 2009; Vogel *et al.*, 2003) or vortex core reversal (Bocklage *et al.*, 2008; Van Waeyenberge *et al.*, 2006). Owing to the photon-in–photon-out technique used in our set-up, there is no charging or magnetic field effect to worry about.

The experiments were carried out at the UE52 beamline at the BESSY II synchrotron at the Helmholtz-Zentrum Berlin (HZB), using the ALICE diffractometer (Grabis *et al.*, 2003) as end-station. The undulator beamline provides X-rays of variable energy and polarization, including circularly polarized light at the resonant energies of the 3*d* transition elements. During the single-bunch operation mode of the synchrotron, the intensity of the undulator is still sufficiently high (about one order of magnitude less compared with multibunch mode) to render time-resolved experiments feasible. The ALICE chamber is a versatile two-circle diffractometer with horizontal scattering geometry, and a broad field and temperature range is accessible at the sample position. Using circularly polarized light in reflection geometry at the element-specific resonant energies, we probe the horizontal, or M_x (collinear with the beam), component of the magnetization (equivalent to the longitudinal MOKE geometry). In this way element-specific information on the static magnetization profile of various magnetic heterostructures is accessible.

For the time-resolved experiments we designed a special sample holder for the ALICE chamber serving the needs for an additional field in the direction perpendicular to the scattering plane and for the high-frequency (HF) supply. A

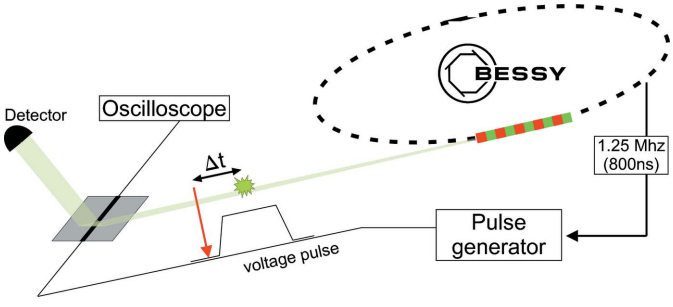

Figure 1
Schematic of the pump–probe set-up. The delay between voltage pulse and photon pulse is varied, and the reflected intensity is measured as a function of delay time.

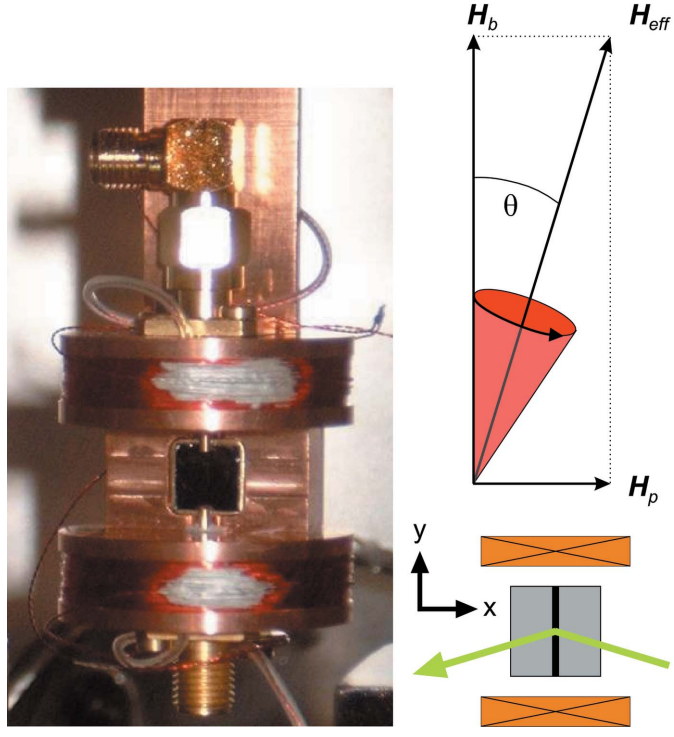

Figure 2
Photograph of the sample holder with coils and HF connectors. The black rectangle is a Si substrate, positioned from the back side. An M8 screw at the top connects the sample holder with the cryostat (upmost part). The right-hand panel is a schematic of the stripline sample geometry with the bias field H_b parallel to the stripline and the pulsed field H_p provided by a current through the stripline perpendicular to it. The vector sum of both fields defines the effective field direction H_{eff}, about which the precessional magnetization dynamics occurs before it is aligned parallel to the H_{eff} axis. In the time-resolved resonant magnetic X-ray scattering experiment the x-component of the precessing magnetization, M_x, is detected as a function of time after pulse excitation.

photograph of the sample holder together with a schematic outline of the set-up is shown in Fig. 2.

This sample holder combines in a convenient way the capabilities of the diffractometer in terms of field, angular and temperature range with the possibility to conduct time-resolved experiments at the very same sample. In order to ensure good thermal conductivity and to minimize temperature drifts the sample holder is fabricated from Cu. It includes a pair of coils to generate a bias field H_b perpendicular to the scattering plane, and SMA connectors to contact the sample to the HF wiring. Two pins serve as electrical contacts by just pressing a sample against them from the back side. These solder-free contacts enable simple and fast sample change from the back side of the sample holder without the necessity of disconnecting any HF wiring. The sample itself is glued onto a small sledge and fixed through an opening from the back side of the sample holder. Owing to its position it is always placed at the center of rotation once the sample holder is aligned, resulting in very short alignment times. A delta electronika constant current source delivers up to 460 mA for the coils, resulting in a maximum bias field of $\sim$100 Oe. However, this field is only used to saturate the sample along the stripline prior to data acquisition, as the heat dissipation of the coils generates a temperature drift and limits the permanent currents to about 250 mA. The sample is a 7 mm $\times$ 7 mm Si substrate with a centered conducting stripline of width 600 µm and length 7 mm as main conducting layer and a magnetic layer deposited on top.

The main parts of the sample holder are sketched in the lower right panel of Fig. 2. Since we use circularly polarized light we are sensitive to the magnetization parallel to the x-direction, thus the magnetic contribution to the reflected signal is $I_m \propto \boldsymbol{\sigma}\cdot\mathbf{M}$, where $\boldsymbol{\sigma}$ denotes the photon helicity and $\mathbf{M}$ is the magnetization vector. The rotatable electromagnet in the ALICE chamber provides a magnetic field H_x parallel to the sample surface and in the scattering plane in order to measure element-selective hysteresis loops for static characterization. A constant current applied through the stripline will then result in a shift of the hysteresis, as the magnetic field generated by the current will add to the external field H_x supplied by the electromagnet. The bias field H_b, on the other hand, induces an easy-axis behavior parallel to the stripline and thus a hard-axis behavior along the x-direction. The fields present at the sample position are shown in the top right panel of Fig. 2. Temporal resolution is obtained using a pump–probe technique during single-bunch operation mode at BESSY II; only one bunch travels in the storage ring, the photons generated arrive in pulses of 50 ps width and a separation of 800 ns, *i.e.* a repetition rate of 1.25 MHz. The synchrotron masterclock provides a trigger signal at this frequency with a fixed yet arbitrary phase to the photons hitting the sample. The photon pulse length sets the upper limit of the time resolution. Any processes that are faster than 50 ps are not accessible with our set-up. For the excitation of the precession the trigger signal from the BESSY masterclock is fed into an HP8130A pulse generator, which serves as a delay station and is controlled *via* a GPIB interface. The output signal is then

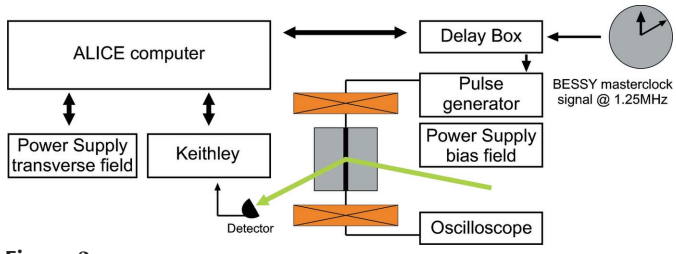

Figure 3
Schematic outline of the electronics for time-resolved experiments. The left part shows the standard ALICE equipment, the right part the electronics set-up for the time-resolved experiments. The double arrows mark GPIB communication.

connected to an AvTech pulse generator, generating a voltage step of length 10 ns and a variable amplitude of up to 10 V with a rise time of 225 ps (10/90). This pulse is delivered to the sample *via* 50 Ω coaxial cables and finally fed into a 20 GHz HP 54110D oscilloscope during the measurements. All cables and electrical feedthroughs used in this set-up are chosen for small damping loss in the frequency range up to 18 GHz to sustain the high-frequency components of the edges of the voltage pulse and to maintain a sharp rise and fall time of the field pulse. This is essential for observing free precessional motion in the sample instead of an adiabatic change of the magnetization vector in response to a change of the field direction. The voltage pulse directly results in a magnetic field pulse at the sample position; the shape of the voltage pulse observed at the scope is a direct measure of the shape of the magnetic field pulse. A schematic of the electronic circuit is shown in Fig. 3.

The reflected intensity is detected by a GaAs photodiode together with a Keithley picoammeter, as a function of delay time. Delay control and data acquisition is carried out *via* the *SPEC* software (Certified Scientific Software, Cambridge, MA, USA; http://www.certif.com/). The delay between the masterclock signal and the voltage pulse at the sample is controlled with the HP8310A *via* a GPIB interface. The minimum step size possible is 10 ps, which is well below the intrinsic length of the photon pulse (50 ps).

For each delay step the signal is integrated over for about 30 s, and a reference signal is measured without applying a current pulse. The latter is important for monitoring the background signal and avoiding stability effects owing to the small size of the sample. As a whole scan takes about half an hour the stability of the sample with respect to the beam is an important issue. For striplines of only 50 µm in width we observed a very noisy signal that we assign to small variations of the sample position with respect to the beam. This resulted in intensity variations of up to 5%, which is in the range of the signal to be measured and prevents any time-resolved scans being taken. Therefore, the width of the stripline should be of the same order as the beam size.

3. Results and discussion

As a test sample we present results of a polycrystalline 25 nm-thick Py layer on top of a 50 nm-thick Cr stripline. The

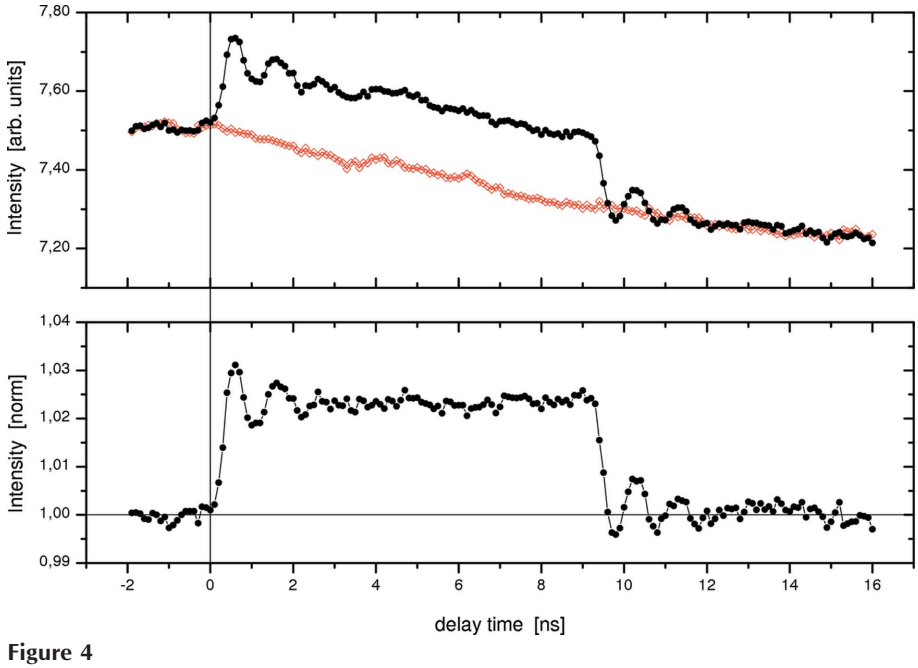

Figure 4
The upper part shows the intensity detected as a function of delay time with (full) and without (open symbols) current pulse. Both intensities drop because of the ring decay. The lower graph shows the same delay scan where the intensity with pulsed excitation is normalized to the one without. The oscillations at the leading and trailing edges are clearly recognized.

structure was deposited on a Si substrate through a mask resulting in a 600 μm-wide stripline. All scans shown in Figs. 4 and 5 were taken at the Fe L_3 resonant edge at an incident and exit glancing angle of 7°. Prior to each delay scan the sample is saturated along the stripline and subsequently the bias field is released to a fixed value. The magnetization is then considered to be aligned along the y-direction, yielding no magnetic asymmetry in the reflected intensity. Subsequently, the change in reflected intensity is monitored as a function of delay time between excitation and probe. Fig. 4 shows a typical result for a bias field of 11.5 Oe and a voltage pulse of 10 V amplitude and 10 ns length, leading to a magnetic field pulse H_p of about 1 Oe.

The overall step in the intensity arises from the magnetic field pulse, and the step height represents the new equilibrium direction for the magnetization being aligned along H_{eff}. In a first approximation this is given by the vector sum of H_b and H_p, neglecting any other contributions (compare the right-hand part of Fig. 2). In this image the angle θ between H_{eff} and H_b can be determined from the intensity change at the step. The change of the direction of the magnetic field with the rising edge of the current pulse leads to damped free precession about H_{eff}. In the reflected intensity we observe the projection of the magnetization precession into the x-direction, which appears as a damped harmonic oscillation. The damped oscillations at both leading and trailing edge of the excitation are clearly visible, lasting for a few nanoseconds. Anisotropies are neglected in this picture but may become important for a more detailed analysis of the data. To prove that the observed oscillations are not by any means a geometric effect, we have changed the photon helicity, bias field direction and current pulse direction, obtaining comparable results in all cases.

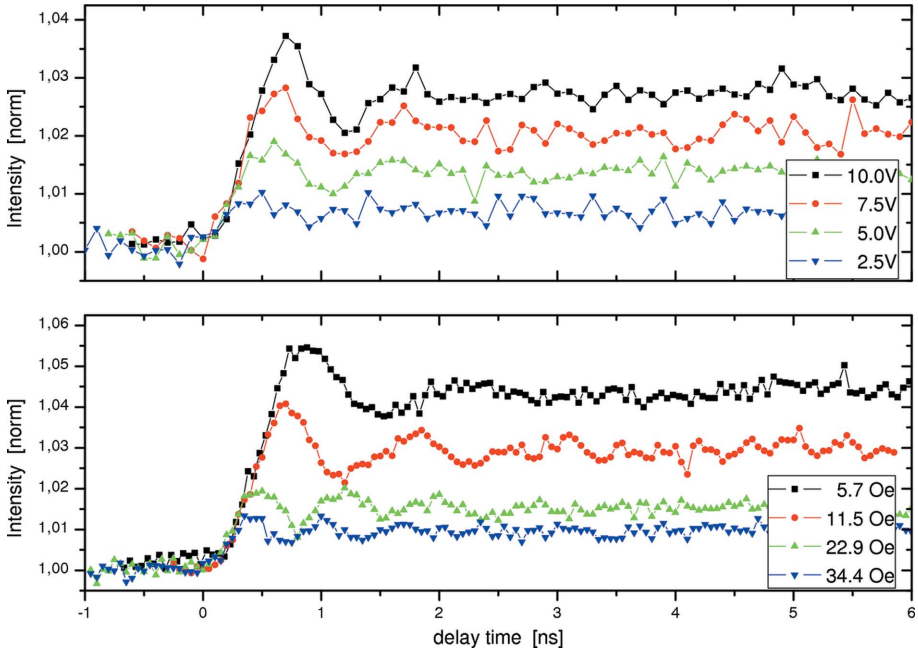

Figure 5
The upper panel shows delay scans at four different amplitudes of the pulsed field at a constant bias field of 11.5 Oe. The lower panel shows the effect of an increasing bias field at a constant pulse field. The change in step height is not linear with the bias field because there is always a constant $H_{eff,x} = H_p$ present.

Delay scans at a fixed bias field of 11.5 Oe for four different pulse amplitudes are shown in the top panel of Fig. 5 at the rising edge of the field pulse. The overall step height decreases with decreasing pulse amplitude as expected since the angle θ between H_{eff} and H_b and the projection of **M** into the x-direction becomes smaller for smaller H_p. This almost linear reduction leads to the assumption that the pulsed field is small compared with the bias field. The lower panel of Fig. 5 shows the effect of different bias fields at fixed pulse amplitude. Again, the step height decreases with increasing bias fields as θ decreases with increasing bias field. The data also clearly show an increasing oscillation frequency, which is expected

for increasing effective field according to the Kittel formula (Kittel, 1996). Finally, in both data sets we notice that the initial slope upon the excitation is similar for all parameters chosen, although the final step height is different. The time where M_x first transits to the new equilibrium increases with the step height. The observed frequencies are in the low GHz regime, which is reasonable for Py. We have obtained equivalent results for the Ni moments in Py when tuning the X-ray energy to the Ni L_3 edge. This proves that, with the set-up described here, we are able to measure element-resolved precessional magnetization dynamics; a detailed analysis of our data will be reported elsewhere.

4. Conclusion and outlook

We have constructed an add-on sample holder for the ALICE chamber, which together with the electronics enables time- and element-resolved experiments in reflection geometry with a time resolution of less than 100 ps. A pulsed magnetic field triggers a magnetization precession $\mathbf{M}(t)$ about a new effective field direction $H_{\rm eff}$, the projection of which into the scattering plane $M_x(t)$ is detected as a damped oscillation after defined time delays. This stroboscopic detection mode allows time scans from 100 ps up to a few nanoseconds. The expected dependencies of the M_x component on both the pulsed magnetic field amplitude and the bias field strength are clearly recognized for a Py thin-film sample. Furthermore, we observe the expected frequency increase for increasing bias field. Future experiments will focus on the magnetization dynamics and damping in multilayer structures and laterally patterned samples. The reflection geometry is ideally suited for these kinds of samples, as the substrate can be chosen arbitrarily, and furthermore depth information is obtained *via* variation of the scattering vector.

We would like to thank Dario Arena and Alexei Nefedov for helpful discussions. This work was supported by the BMBF Verbundforschung (05KS7PC1), which is gratefully acknowledged. We are also thankful to HZB Berlin supported by BMBF for travel funds under 05ES3XBA/5.

References

Arena, D. A., Ding, Y., Vescovo, E., Zohar, S., Guan, Y. & Bailey, W. E. (2009). *Rev. Sci. Instrum.* **80**, 083903.
Bailey, W. E., Cheng, L., Keavney, D. J., Kao, C.-C., Vescovo, E. & Arena, D. A. (2004). *Phys. Rev. B*, **70**, 172403.
Bauer, M., Lopusnik, R., Fassbender, J. & Hillebrands, B. (2000). *Appl. Phys. Lett.* **76**, 2758–2760.
Beaurepaire, E., Merle, J.-C., Daunois, A. & Bigot, J.-Y. (1996). *Phys. Rev. Lett.* **76**, 4250–4253.
Bland, J. & Heinrich, B. (2005). *Ultrathin Magnetic Structures III – Fundamentals of Nanomagnetism.* Berlin: Springer.
Bocklage, L., Krüger, B., Eiselt, R., Bolte, M., Fischer, P. & Meier, G. (2008). *Phys. Rev. B*, **78**, 180405.
Dürr, H., Eimüller, T., Elmers, H.-J., Eisebitt, S., Farle, M., Kuch, W., Matthes, F., Martins, M., Mertins, H.-C., Oppeneer, P., Plucinski, L., Schneider, C., Wende, H., Wurth, W. & Zabel, H. (2009). *IEEE Trans. Magn.* **45**, 15–57.
Farle, M. (1998). *Rep. Prog. Phys.* **61**, 755.
Gerrits, T., Silva, T. J. & Rasing, T. (2006). *Rev. Sci. Instrum.* **77**, 034704.
Gerrits, T., van den Berg, H. A. M., Hohlfeld, J., Bar, L. & Rasing, T. (2002). *Nature (London)*, **418**, 509–512.
Grabis, J., Nefedov, A. & Zabel, H. (2003). *Rev. Sci. Instrum.* **74**, 4048–4051.
Heinrich, B. (2008). *Springer Tracts Mod. Phys.* **227**, 185.
Hubert, A. & Schäfer, R. (1998). *Magnetic Domains.* Berlin: Springer.
Kaiser, A., Wiemann, C., Cramm, S. & Schneider, C. M. (2009). *J. Phys. Condens. Matter*, **21**, 314008.
Kalarickal, S. S., Krivosik, P., Wu, M., Patton, C. E., Schneider, M. L., Kabos, P., Silva, T. J. & Nibarger, J. P. (2006). *J. Appl. Phys.* **99**, 093909.
Kittel, C. (1996). *Introduction to Solid State Physics.* New York: Wiley.
Kläui, M. (2008). *J. Phys. Condens. Matter*, **20**, 313001.
Martin, T., Woltersdorf, G., Stamm, C., Dürr, H. A., Mattheis, R., Back, C. H. & Bayreuther, G. (2008). *J. Appl. Phys.* **103**, 07B112.
Martin, T., Woltersdorf, G., Stamm, C., Dürr, H. A., Mattheis, R., Back, C. H. & Bayreuther, G. (2009). *J. Appl. Phys.* **105**, 07D310.
Neudert, A., McCord, J., Chumakov, D., Schäfer, R. & Schultz, L. (2005). *Phys. Rev. B*, **71**, 134405.
Nibarger, J. P., Lopusnik, R., Celinski, Z. & Silva, T. J. (2003). *Appl. Phys. Lett.* **83**, 93–95.
Raabe, J., Quitmann, C., Back, C. H., Nolting, F., Johnson, S. & Buehler, C. (2005). *Phys. Rev. Lett.* **94**, 217204.
Shpyrko, O. G., Isaacs, E. D., Logan, J. M., Feng, Y., Aeppli, G., Jaramillo, R., Kim, H. C., Rosenbaum, T. F., Zschack, P., Sprung, M., Narayanan, S. & Sandy, A. R. (2007). *Nature (London)*, **447**, 68–71.
Silva, T. J., Lee, C. S., Crawford, T. M. & Rogers, C. T. (1999). *J. Appl. Phys.* **85**, 7849–7862.
Stamm, C., Kachel, T., Pontius, N., Mitzner, R., Quast, T., Holldack, K., Khan, S., Lupulescu, C., Aziz, E. F., Wietstruk, M., Dürr, H. A., Eberhardt, W., Gerrits, T., van den Berg, H. A. M., Hohlfeld, J., Bar, L. & Rasing, T. (2007). *Nat. Mater.* **418**, 509–512.
Van Waeyenberge, B., Puzic, A., Stoll, H., Chou, K. W., Tyliszczak, T., Hertel, R., Fähnle, M., Brückl, H., Rott, K., Reiss, G., Neudecker, I., Weiss, D., Back, C. H. & Schütz, G. (2006). *Nature (London)*, **444**, 461–464.
Vogel, J., Kuch, W., Bonfim, M., Camarero, J., Pennec, Y., Offi, F., Fukumoto, K., Kirschner, J., Fontaine, A. & Pizzini, S. (2003). *Appl. Phys. Lett.* **82**, 2299–2301.
Wernsdorfer, W., Orozco, E. B., Hasselbach, K., Benoit, A., Barbara, B., Demoncy, N., Loiseau, A., Pascard, H. & Mailly, D. (1997). *Phys. Rev. Lett.* **78**, 1791–1794.